

# Helioseismic insights into the generation and evolution of the Sun's internal magnetic field

Anne-Marie Broomhall<sup>id</sup> and René Kiefer

Centre for Fusion, Space and Astrophysics, Department of Physics,  
University of Warwick, CV4 7AL  
email: [a-m.broomhall@warwick.ac.uk](mailto:a-m.broomhall@warwick.ac.uk)

**Abstract.** Properties of helioseismic acoustic oscillations (p modes) are modified by flows and magnetic fields in the solar interior, with frequencies, amplitudes and damping rates all varying systematically through the solar cycle. Crucially, now, we have a long enough baseline of helioseismic data to compare of the different activity cycles. We review recent efforts along these lines, from the impact of near-surface magnetic fields on p-mode frequencies to the evolution of the torsional oscillation and meridional circulation. We show that each activity cycle for which we have helioseismic data is slightly different in terms of the relationship between p mode frequencies and atmospheric proxies of activity, and in terms of the rotation and meridional circulation flows. However, many challenges remain, crucially including our ability to constrain flows and magnetic fields in the deep solar interior.

**Keywords.** Sun: activity, Sun: helioseismology, Sun: interior, Sun: magnetic fields, Sun: oscillations, Sun: rotation

---

## 1. Introduction

Helioseismology uses the Sun's resonant oscillations to infer conditions beneath the solar surface. At any point in time there are thousands of acoustic oscillations travelling throughout the solar interior. These oscillations sample different but overlapping regions of the solar interior and so by studying the properties of these oscillations, and using models, we can build up a profile of the inside of the Sun. For example, we can learn about how temperature and rotation vary with depth and we can even use helioseismology to learn about the composition of the Sun. The acoustic oscillations, upon which we will focus here, are referred to as p modes as the main restoring force is a pressure differential.

We describe helioseismic oscillations in terms of spherical harmonics, which are characterised by three main “quantum” numbers. The first of these is the spherical harmonic degree, or  $\ell$ , which specifies the total number of nodes present at the surface. As an oscillation travels inwards, the temperature, and therefore the sound speed, increases so, unless the oscillation is travelling perfectly radially, it will be refracted until it returns to the surface. The depth a mode travels to before being completely refracted depends on the angle it's travelling inwards at near the surface and this varies as a function of  $\ell$ : the lowest- $\ell$  modes travel radially, or nearly radially, and so penetrate deeper in the solar interior than high- $\ell$  modes, which only sample the near surface regions. It is this difference in the depth of the “lower-turning point” that allows us to build up profiles of the solar interior.

The second number we use to describe the spherical harmonic structure of the modes is the azimuthal degree or  $m$ , and this describes the number of nodes round the equator. Again showing similarities to quantum mechanics, if the Sun were completely symmetric, each one of the  $m$  components of a mode would have the same frequency. However

asymmetries, like rotation and other flows, split the frequencies of the different  $m$  components, with the magnitude of that splitting providing information about the asymmetries responsible.

The final number used to describe the modes is the radial degree,  $n$ . As the name suggests,  $n$  describes the number of nodes in the radial direction, with the frequency of the oscillations increasing as a function of  $n$ .

As already mentioned, the modes, are refracted in the solar interior until they return towards the surface. When the modes reach the surface again they are reflected by the sharp drop in density and the radius at which reflection takes place depends on the length scale of the mode in comparison to the density scale height and, therefore, on mode frequency. More specifically, the high-frequency modes are reflected further out than low-frequency modes. Another way of thinking of this is that, for a particular radius, there is a specific acoustic cut-off frequency, where all modes below that frequency have already been reflected and all modes above that frequency are transmitted.

Helioseismic observations can be made using both Doppler velocity and intensity. Then there are two main branches of helioseismology: global and local. Global helioseismology studies the natural resonant oscillations that cause the Sun to oscillate as a whole and itself can be split into two sub-branches. There is unresolved, Sun-as-a-star helioseismology, whose observations are only sensitive to low- $\ell$  modes or those with the largest horizontal length scales. This is because, for unresolved observations, the forwards and backwards motions associated with higher- $\ell$  modes cancel each other out, meaning the modes are not visible. Sun-as-a-star helioseismic data can easily observe oscillations with  $\ell \leq 3$ , and modes with  $\ell = 4$  and 5 are just about visible in some data sets (e.g. Chaplin *et al.* (1996); Lund *et al.* (2014)). However, it is worth remembering that these low- $\ell$  modes are the ones that travel deepest in the solar interior. A number of long-baseline Sun-as-a-star datasets now exist, which readily allow solar-cycle helioseismic studies to be performed. These include the Birmingham Solar Oscillations Network (BiSON), which has been making Doppler velocity observations since the 1970s, the Global Oscillations at Low Frequency (GOLF) instrument, which also makes Doppler velocity observations and has been operational since its host spacecraft, the Solar and Heliospheric Observatory (SoHO) was launched in 1995, and the Variability of Solar Irradiance and Gravity Oscillations (VIRGO) instrument, which is also onboard SoHO and makes intensity observations. Resolved observations use spatial filters to allow much higher- $\ell$  modes to be observed. There are also long-baseline resolved observations of global modes available, which are suitable for solar cycle studies, including those from the Global Oscillations Network Group (GONG), which produces Doppler velocity data for global modes with  $0 \leq \ell \leq 200$  going back to 1996. Other commonly used instruments include the Michelson Doppler Imager (MDI), which observed from the launch of SoHO until 2011, and the Helioseismic and Magnetic Imager (HMI), which is onboard the Solar Dynamics Observatory (SDO) and was launched in 2010. Using the overlap to scale the data, it is common practice to combine MDI and HMI results when studying solar cycle variations in the p modes. Further details on global helioseismology can be found in Basu (2016).

Local helioseismology studies waves in localised patches of the surface and is able to infer conditions and parameters, such as those used to describe localised flows, say beneath a sunspot. This too has different branches and methodologies based on the different observational techniques. Ring-diagram analysis is most akin to global helioseismology, only observations are made on small “tiles” and Fourier transforms are performed in 3 dimensions, giving power spectra as a function of two horizontal wavenumbers,  $k_x$  and  $k_y$ , as well as frequency. The power appears in rings, hence the name, that are shifted and distorted, in the  $x$  and  $y$  directions by flows and in frequency by localised

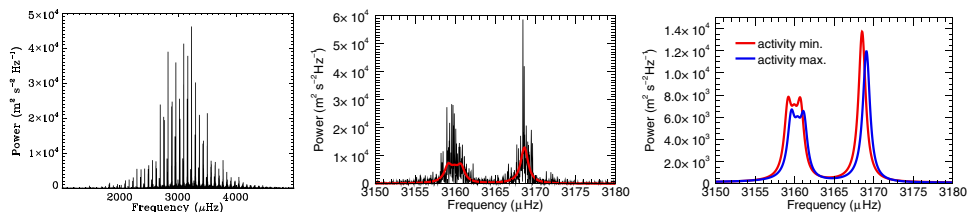


**Figure 1.** Left: spectrum obtained from 365 d of BiSON Sun-as-a-star Doppler velocity data. Middle: close up of an  $\ell=2$  and an  $\ell=0$  mode in this spectrum. The red line is the fitted Lorentzian profiles. Right: comparison of the profiles fitted to these two modes at activity maximum and activity minimum.

changes in the wave speed. The second technique frequently used in helioseismology is known as time-distance helioseismology. Here, the travel time of a wave between two surface locations is determined using cross-correlation techniques. Inhomogeneities, such as flows, magnetic fields and anisotropies in the sound speed affect the travel time and inversions are performed to determine the properties of the inhomogeneity. GONG, MDI and HMI are all frequently used in local helioseismic studies. Further details on local helioseismology can be found in [Gizon & Birch \(2005\)](#).

We now move on to describe how the parameters of the global p modes vary through the solar cycle (in Section 2) before a discussion on flows in the solar interior that play important roles in many dynamo models (in Section 3) and finally we will describe how these flows vary through the solar cycle.

## 2. Solar cycle variations in p mode parameters

When we observe global p modes we tend to make relatively long observations of the Sun, of the order of months to years, and then perform some form of Fourier-like transform to make a power spectrum. The left panel of Figure 1 shows an example of one such power spectrum obtained from 365 d of Sun-as-a-star Doppler velocity observations, made by BiSON ([Davies \*et al.\* \(2014\)](#); [Hale \*et al.\* \(2016\)](#)). Each one of the peaks you can see is a different mode of oscillation. If we zoom in on just two modes, as shown in the middle panel of Figure 1, we can see that the mode peaks have structure because the modes behave like damped harmonic oscillators. We can, therefore, fit asymmetric Lorentzian profiles to the peaks in order to determine mode parameters, such as frequencies, powers and damping rates (which are indicated by the width of the peaks). These parameters all vary through the Sun's magnetic activity cycle. In the right panel of Figure 1, we can see a comparison between the mode profiles that were fitted to the two p modes shown in the middle panel at solar maximum and minimum. The variations in frequency and maximum power of the profiles are easily visible. Less easy to discern is the variation in the width of these profiles, but it is there nonetheless.

Figure 2 shows the average shift in frequency of p modes as a function of time. A scaled and shifted version of the 10.7 cm flux is also plotted for comparison. While the zero point is somewhat arbitrary, the 11 yr solar cycle is clearly visible in frequency shifts. The p-mode frequencies increase as the solar magnetic field increases, with  $\ell=0$  p modes at about 3000  $\mu\text{Hz}$  experiencing a shift of about 0.4  $\mu\text{Hz}$  between cycle minimum and maximum. The causes of these variations can broadly be split into two categories: direct and indirect effects. The direct effects involve the Lorentz force, which provides an additional restoring force, thereby increasing the frequency of the modes. The indirect effects involve changes in the properties of the cavity in which the modes are trapped, for example, the size of the acoustic cavity.

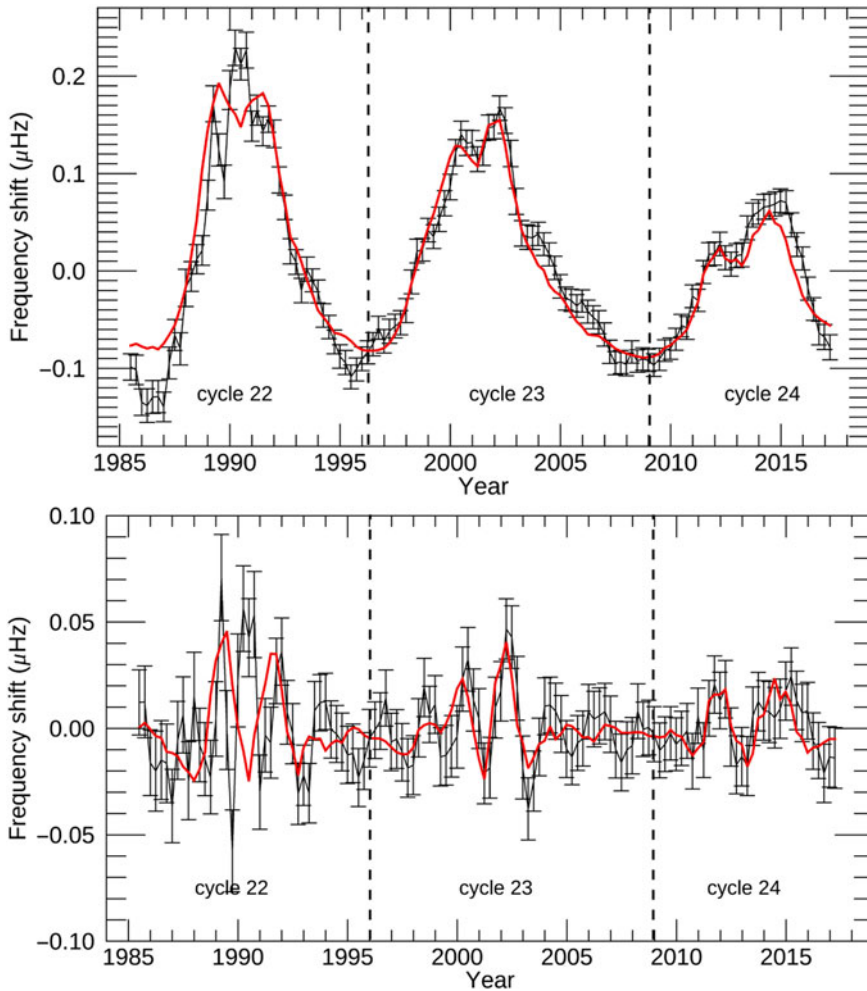


**Figure 2.** Top: average shift in p-mode frequencies between cycle minimum and cycle maximum (black data points). Red line shows a scaled version of the 10.7 cm flux for comparison. Bottom: frequency-shift residuals that remain once a smoothed version of the frequency shifts in the top panel has been subtracted (black data points). Red line shows the 10.7 cm flux residuals, obtained by the same process.

The frequency-shift residuals plotted in the bottom panel of Figure 2 were obtained by removing a smooth 11 yr variation from the frequency-shift data (obtained using a box-car smoothing with a 3 yr window). There is evidence for the “quasi-biennial oscillation (QBO)” in the residuals, which are highly correlated with those seen in atmospheric proxies of solar activity, including the 10.7 cm flux. In fact, the QBO is seen in a large number of activity proxies [Bazilevskaya et al. \(2014\)](#). We note that the amplitude of the observed QBO varies with time, being at a maximum close to solar maximum. This too is a feature of the QBO seen in other activity proxies. The presence of the QBO in helioseismic data provides a link between the signal seen in atmospheric activity proxies with the magnetic field in the solar interior. The challenge now is to use this signal to gain insights into the origin and structure of the magnetic field responsible for the QBO.

It is also interesting to compare the frequencies observed at different times in the solar cycle. Figure 3 shows the difference in p-mode frequencies observed at cycle minimum

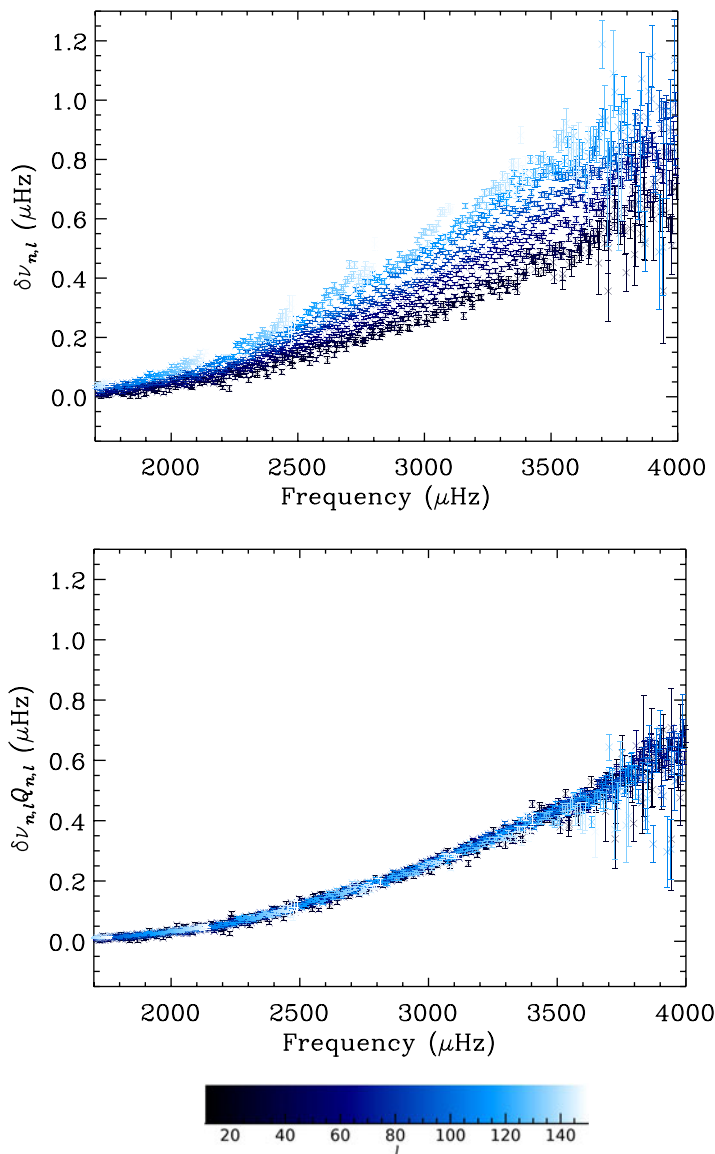


**Figure 3.** Top: frequency shifts observed when comparing observations from cycle maximum and cycle minimum. Bottom: inertia corrected frequency shifts observed when comparing observations from cycle maximum and cycle minimum. Modified from [Broomhall \*et al.\* \(2017\)](#).

and cycle maximum. The size of the frequency shift is dependent on both the degree and frequency of the mode. The degree dependence can be understood in terms of mode inertia [Christensen-Dalsgaard & Berthomieu \(1991\)](#), which is lower for the high- $\ell$  modes than the low- $\ell$  modes, meaning that the high- $\ell$  modes are more easily perturbed. Normalizing by the mode inertia removes the degree dependence, leaving something that is dependent on frequency alone (as can be seen in [Figure 3](#)). The strong frequency dependence, with little or no dependence on degree, is taken to imply that most of frequency changes are caused by effects confined to near-surface layers ([Gough \(1990\)](#); [Libbrecht & Woodard \(1990\)](#)). The higher the mode frequency, the higher the upper turning point of the mode (defined as the radius at which the modes are reflected back into the solar interior).

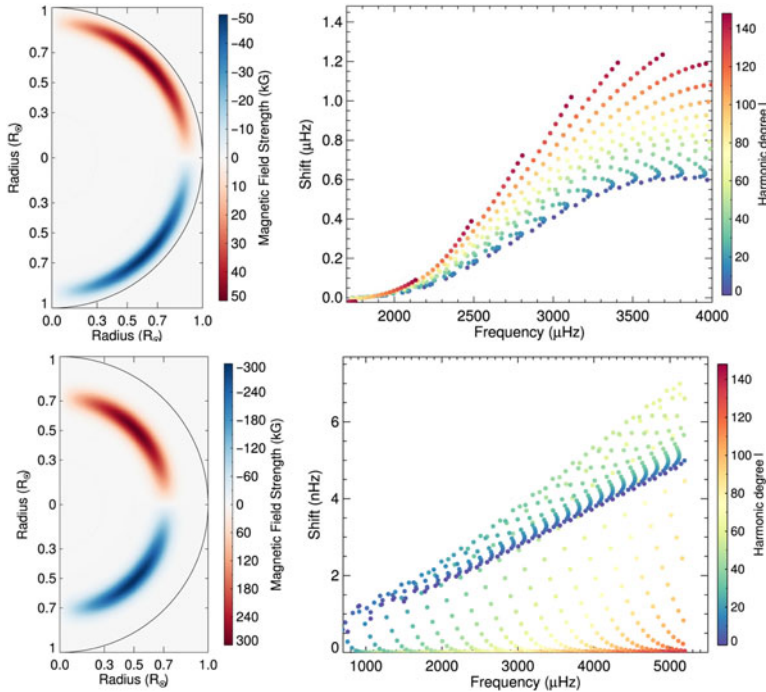


**Figure 4.** Top, left: dipolar, near-surface magnetic field, used to simulate the impact of a magnetic field on the mode frequencies at cycle maximum. To simulate the impact of a magnetic field on the modes at cycle minimum the maximum field strength was reduced by 10 kG. Top, right: shift in frequency between the simulated cycle maximum and cycle minimum. First published in Kiefer & Roth (2018). Bottom, left: Strong dipolar magnetic field introduced at the base of the convection zone. Bottom, right: Frequency shift caused by introduction of field shown in bottom, left panel.

Therefore, if the magnetic perturbation occurs in the near-surface region, a region in which low-frequency modes may not penetrate but high-frequency modes do, it stands to reason that the perturbation has a larger impact on high-frequency modes than low-frequency modes. Latitudinal inversions, such as those performed in Howe *et al.* (2002), show that the latitudinal structure of the perturbation very closely follows that of the well-known butterfly diagram.

Kiefer *et al.* (2017) and Kiefer & Roth (2018) demonstrated that the observed frequency shift can be replicated by modelling direct and indirect effects: A toroidal magnetic field is constructed and, by varying its strength but maintaining the same structure, used to simulate the solar cycle. These magnetic fields are then used to perturb the mode frequencies and the difference in mode frequency between the two states is determined. Figure 4 shows the impact of a change in near-surface field strength of 10 kG, when the field is dipolar. It is clear that this figure closely follows the form seen in the real data (i.e. as seen in Figure 3). Kiefer & Roth (2018) also tried putting a very strong dipolar field of 300 kG at the base of the convection zone. As can be seen in Figure 4, this produced a tiny shift of the order of nHz, which can be compared to the  $\mu$ Hz shift produced by the much smaller near-surface field. This indicates that it is going to be extremely difficult to detect the impact of any field at the base of the convection zone. It is, however, a worthy goal, given that many believe this region to be the seat of the solar dynamo.

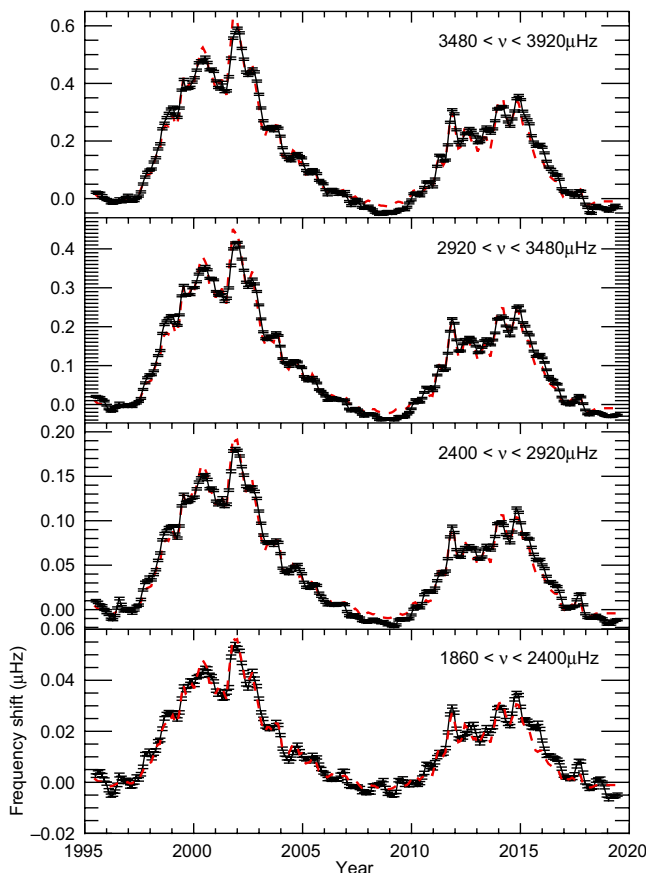


**Figure 5.** Frequency shifts as a function of time for  $0 \leq \ell \leq 150$  modes observed by GONG. The frequency shift data (black data points) have been averaged over four different frequency ranges. For comparison, scaled and shifted versions of the 10.7 cm flux have been included.

### 2.1. Solar cycle comparisons

Arguably one of the most interesting, and least understood, features of the solar cycle is its variability: each solar cycle is different to the next. Even though it is often referred to as the the 11 yr solar cycle, the length of each cycle varies, usually lying somewhere in the region of 9 – 14 yr [Hathaway \(2015\)](#). The amplitude of an activity cycle also varies from one cycle to the next, making accurate predictions of the strength and timing of solar maximum notoriously difficult. Although relatively new on the scene, compared to say sunspot records, helioseismology now has continuous observations spanning decades, meaning we even have data covering a full Hale cycle (which consists of two solar cycle and accounts for the fact that there is a polarity reversal after each 11 yr cycle). This means that we can begin to compare activity cycles to determine if we can discern what causes the cycle-to-cycle variability.

It is common, when looking at solar cycle variation in p-mode parameters to average the observed variation over a range of frequencies. Figure 5 shows two full cycles of frequency shifts as seen with GONG, where the frequency shifts are averaged over four frequency ranges. This was also the approach taken by [Basu \*et al.\* \(2012\)](#), [Salabert \*et al.\* \(2015\)](#), and [Howe \*et al.\* \(2017\)](#), when looking at frequency shifts in low- $\ell$  modes, seen in Sun-as-a-star data. Each of these authors showed that there is a change in the relationship

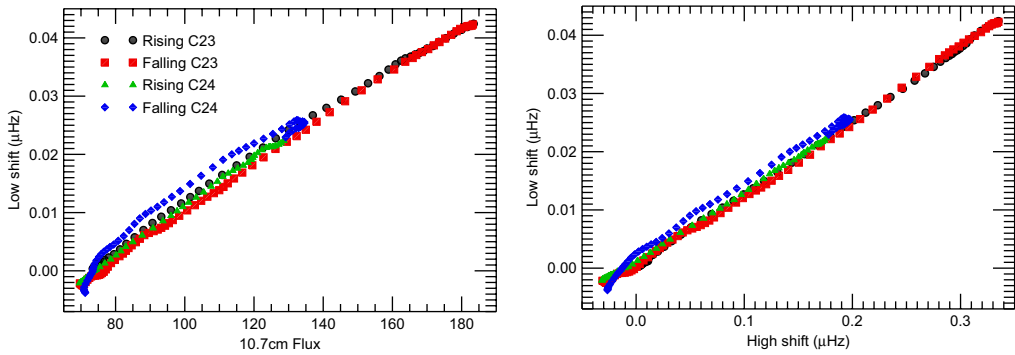


**Figure 6.** Left: frequency shift in the low-frequency band from Figure 5, which extends between  $1860 \leq \nu \leq 2400 \mu\text{Hz}$ , as a function of 10.7 cm flux (measured in RFU). Right: Frequency shift in the low-frequency band as a function of the frequency shift in the high-frequency band, which extends between  $2920 \leq \nu \leq 3480 \mu\text{Hz}$ . The difference colours indicate the different phases of different cycles, as indicated in the legend.

between low-frequency, low- $\ell$  modes and atmospheric activity proxies between cycles 23 and 24, which resulted in far smaller changes in frequency through the solar cycle than expected and a far lower correlation with atmospheric proxies than seen in previous cycles. However, as can be seen in the bottom panel of Figure 5, a definite solar cycle variation is observed for the low-frequency medium- $\ell$  modes. Nevertheless, as shown in Howe *et al.* (2018a), there is still evidence for a small but systematic and significant cycle-to-cycle variation in intermediate- $\ell$  frequency shifts, with solar cycle 24 showing a shift that was around 10% larger for the same change in atmospheric activity proxy as was observed in cycle 23. This cycle-to-cycle variation is also evident in Figure 6, which directly compares the intermediate- $\ell$  low-frequency-range frequency shifts, as shown in the bottom panel of Figure 5, with the 10.7 cm flux. The activity cycles are offset from one another, as are the rising and falling phases from each individual cycle, indicating the change in relationship between atmospheric and interior activity proxies. Interestingly, this same behaviour can be seen when comparing the low-frequency-range shifts with the frequency shifts observed in a higher frequency band (e.g. here the  $2920 < \nu < 3480 \mu\text{Hz}$  range was used). This is likely to be related to the upper turning point of the modes, which is further out for higher mode frequencies. Thus we can speculate that the cycle-to-cycle change is occurring in the layer containing the upper turning points of the low-frequency modes. For example, one explanation, proposed by Basu *et al.* (2012), is that the layer responsible for the magnetic perturbation has become thinner between cycles 23 and 24, meaning that in cycle 24 the low-frequency modes penetrate less far into the perturbation, if at all, and are thus less affected by the magnetic field.

## 2.2. Variations in other $p$ -mode parameters

As already mentioned, it is not just the mode frequencies that vary with time: mode powers and damping rates also show solar cycle variations (see Kiefer *et al.* (2018), and references therein). The top row of Figure 7 shows the variation in time of mode widths, which are defined as the widths of the Lorentzian profiles like those plotted in Figure 1. These results were obtained using GONG data but the results are consistent with those obtained using Sun-as-a-star data. The mode widths are proportional to mode damping rates and are observed to vary in phase with the solar activity, meaning the damping rates are highest at solar maximum. The powers, defined as the integrated area under the Lorentzian curves plotted in Figure 1, vary in anti-phase with the solar cycle, meaning the

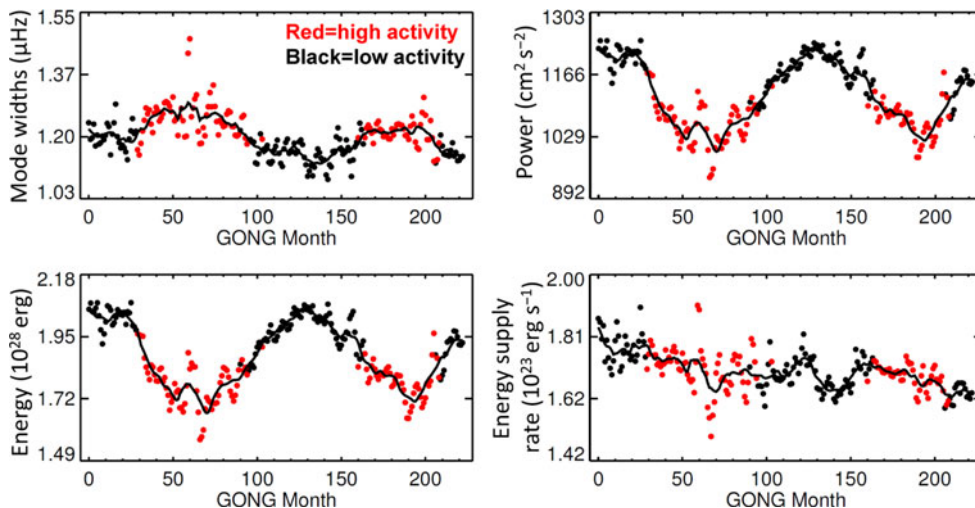


**Figure 7.** Top, left: variation in mode width, which is proportional to damping rate, as a function of time. Top, right: variation in mode power as a function of time. Bottom, left: variation in mode energy as a function of time. Bottom, right: variation in the rate at which energy is supplied to modes as a function of time. Adapted from Kiefer *et al.* (2018).

powers are at a minimum at solar maximum. The mode energies are directly proportional to the mode powers and so they, too, vary in anti-phase with the solar cycle (e.g. Goldreich *et al.* (1994)). The mode energies and damping rates can then be combined to determine the rate at which energy is supplied to the mode (e.g. Goldreich *et al.* (1994)), which is found to be approximately constant with time. We note that the results plotted in Figure 7 require numerous corrections to the data to account for e.g. the fill of the data, but the results are consistent with those found by Keith-Hardy *et al.* (2019), who perform an alternative correction.

### 3. Flows in the solar interior and their relationship with magnetic activity

As already mentioned, the separation in frequency of the different  $m$  components can be used to determine the internal rotation profile of the solar interior. Helioseismology revealed that the differential rotation pattern observed on the surface of the Sun, whereby the equator rotates faster than the poles, extends throughout the outer  $\sim 30\%$  of the solar interior, down to the base of the convection zone (see e.g. (Basu 2016, Basu, 2016)). At the base of the convection zone there is a switch to solid body rotation, resulting in a narrow shear layer known as the tachocline. The tachocline is important in many dynamo models of the Sun, as it is often regarded as the location where the magnetic field is generated and maintained (e.g. Charbonneau (2010)).

The rotation profile of the solar interior does not remain constant through the solar cycle. One such temporal variation is known as the torsional oscillation, which is highlighted by subtracting the mean rotation profile from the rotation profile observed at a specific time. This can be done for different depths in the solar interior allowing a profile of the variation to be inferred. Figure 8 shows the torsional oscillation at  $0.99 R_{\odot}$ . Coherent bands of faster than average and slower than average rotation are clearly visible. The bands of faster than average rotation coincide with the inner edge of the wings on a traditional butterfly diagram but can be traced back to well before a cycle starts and possibly covering the outer edge of the previous cycle. We note that this flow was substantially faster in cycle 24 than cycle 23. The equatorward branch of the new activity

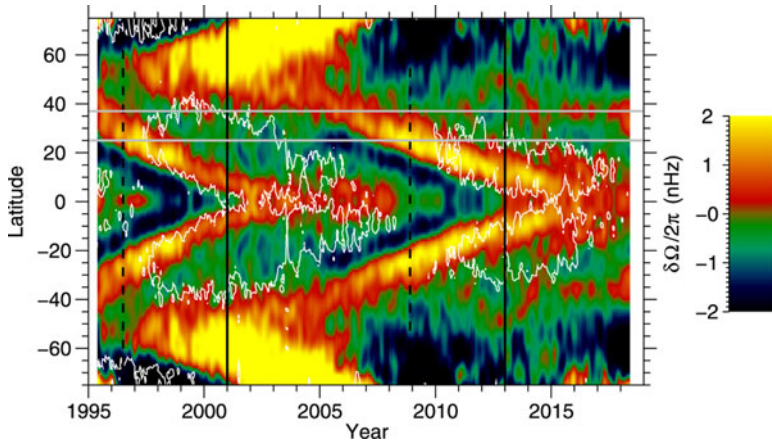


**Figure 8.** Torsional oscillations observed at  $0.99 R_{\odot}$ , obtained using regularized least squares inversions of GONG, MDI and HMI data. The vertical dashed line indicates solar minimum, while the solid vertical lines indicate solar maximum. The white contours, which indicate the locations of the surface magnetic flux at 10% of the maximum level, allow comparison with the butterfly diagram. Originally published in [Howe \*et al.\* \(2018b\)](#).

cycle can just about be seen, but was still relatively weak at the time this figure was published. A poleward branch of faster than average rotation can also be seen from the beginning of cycle 23. Although hard to see in Figure 8, a similar band is present in cycle 24 but it is far weaker. [Kosovichev & Pipin \(2019\)](#) reveal zones of deceleration of the torsional oscillation that originate at high latitudes near the base of the convection zone and migrate towards the surface. They suggest that the deceleration is caused by magnetic field and thus the results are consistent with magnetic dynamo waves, as predicted by Parker's dynamo theory [Parker \(1955\)](#).

Another flow that is important in dynamo models is the meridional flow. As the name suggests, a meridional flow is the circulation of plasma in the meridional plane or perpendicular to rotation. The meridional flow is an important component of flux-transport dynamo models as it is presumed to carry flux from old active regions towards the poles, where it is subducted to the base of the convection zone and transported back towards the equator (see e.g. [Charbonneau \(2010\)](#), for a review). Furthermore, the strength and timescale of the meridional flow is believed to determine the strength and timescale of the Sun's activity cycle, although many models disagree on the exact impact of these parameters. Detecting the near-surface flow is relatively straightforward (e.g. [Giles \*et al.\* \(1997\)](#)). However, as soon as we try and go deeper the uncertainties increase substantially (e.g. [Mitra-Kraev & Thompson \(2007\)](#)): The modes used to make these inversions simply are not sensitive enough to the deeper layers of the Sun because of the high sound speed there. Of course mass conservation indicates that there must be a return flow but results describing the return flows remain controversial.

Figure 9 shows three examples of recently published results on meridional flows (we note that these are not the only three published recently but have been selected because they have plotted their results in a similar manner, making comparison easier). Each uses a slightly different methodology and each produces a different result. [Mandal \*et al.\* \(2018\)](#) find a single cell meridional flow pattern, with a return flow at a depth of  $0.78 R_{\odot}$ . [Chen & Zhao \(2017\)](#), on the other hand, find a double cell structure, with an equatorward flow found between about  $0.82$  and  $0.91 R_{\odot}$  for low latitude areas and between about  $0.85$  and  $0.91 R_{\odot}$  for higher latitude areas. This equatorward flow is sandwiched between two poleward flows. While [Böning \*et al.\* \(2017\)](#) demonstrate that observations are consistent

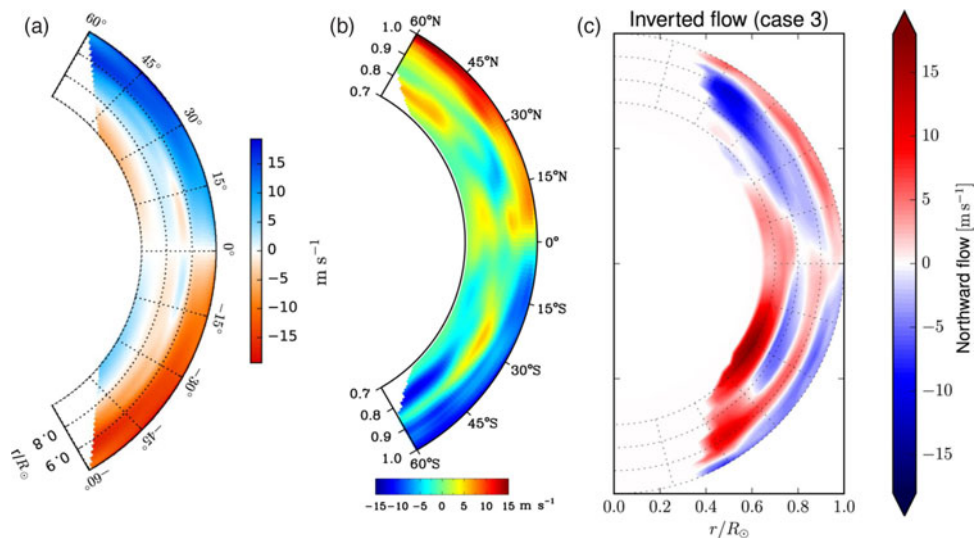


**Figure 9.** (a) Meridional flow inferred by Mandal *et al.* (2018). (b) Meridional flow inferred by Chen *et al.* (2017). (c) Meridional flow inferred by Böning *et al.* (2017).

with both single- and multi-cell meridional flow profiles, but find a much shallower return flow than that observed by Mandal *et al.* (2018). We note that both Chen *et al.* (2017) and Mandal *et al.* (2018) use HMI data, albeit covering slightly different epochs, while Böning *et al.* (2017) use GONG data. All use relatively long data sets, covering six years or more, in order to improve precision at the greater depths needed to study the equatorward meridional flow. However, shorter time series can be used to study solar cycle variations in the near-surface meridional flow.

For example, a recent study by Komm *et al.* (2018) demonstrated that there are evolving bands of faster than average and slower than average meridional flow (just as the torsional oscillation comprises of faster and slower than average rotation). One such band of faster than average meridional flow was observed to migrate towards the equator between the maxima of cycles 23 and 24, meaning that these faster than average meridional flows can be regarded as precursors to the appearance of magnetic field on the surface. In cycle 23, the fast flows were observed at 30 degrees approximately 2 yr before the surface activity from cycle 24 was observed. A new band of fast meridional flow reached 30 degrees in late 2016 – early 2017, implying that we may expect to observe the new cycle in late 2019 – early 2020. The fast flow is sandwiched between bands of slower than average rotation, each of which can be associated with a particular activity cycle, and the first hint of the slow meridional flow associated with cycle 25 appeared in 2016. Komm *et al.* also compare each fast flow with the slow flow preceding it and find that the difference is larger by around a factor of two for cycle 24 compared to the upcoming cycle 25. Liang *et al.* (2018) observed a significant reduction in travel time shifts in cycle 24 but only in the northern hemisphere, this implies a rapid decrease in poleward flows with increasing depth. This north-south asymmetry was not present in cycle 23 and so could provide a hint as to why the cycle 24 was so weak.

#### 4. Summary

Numerous challenges remain in helioseismology and these challenges impact far beyond the Sun. For example, with the current growth of asteroseismology, it will become increasingly important to understand the inner workings of our closest star. Helioseismic results

can provide important constraints not only for models of solar and stellar structure and evolution but also solar and stellar dynamo models. Helioseismology has already provided information vital for the construction of solar dynamo models including, but not limited to, the depth and extent of the tachocline, the rotation profile of the solar interior and the near-surface meridional circulation profile. However, perhaps one area where we can only now make substantial progress is in the comparison of different activity cycles. Can we determine why cycles are so different and what role do changes in the internal flow speeds play?

Dynamo models would greatly benefit from further constraints on the deep solar interior. The deep component of the meridional flow also remains uncertain, with seemingly small changes in methodology resulting in important changes in the inferred rotation profile. Resolving this issue is certainly one of the biggest current challenges facing helioseismologists and yet we are limited by the inherent insensitivity of p modes to the deep solar interior. For the same reason the impact on p modes of magnetic fields at the base of the convection zone is expected to be minuscule (although we should remember that novel analysis techniques have provided a hint in this regard, e.g. [Baldner & Basu \(2008\)](#)). Perhaps gravity modes will play an important role in constraining our understanding of the deep solar interior, and yet the quest to unequivocally detect gravity modes remains frustratingly ongoing.

## References

- Baldner, Charles S. & Basu, Sarbani 2008, *ApJ*, 686, 1349
- Basu, Sarbani, Broomhall, Anne-Marie, Chaplin, William J. & Elsworth, Yvonne 2012, *ApJ*, 758, 43
- Basu, Sarbani 2016, *LRSP*, 13, 2
- Bazilevskaya, G., Broomhall, A.-M., Elsworth, Y. & Nakariakov, V. M. 2014, *Space Sci. Rev.*, 186, 359
- Böning, Vincent G. A., Roth, Markus, Jackiewicz, Jason & Kholikov, Shukur 2017, *ApJ*, 845, 2
- Broomhall, A. -M. 2017, *Sol. Phys.*, 292, 67
- Chaplin, W. J., Elsworth, Y., Howe, R., Isaak, G. R., McLeod, C. P., Miller, B. A. & New, R. 1996, *MNRAS*, 280, 1162
- Charbonneau, Paul 2010, *LRSP*, 7, 3
- Chen, Ruizhu & Zhao, Junwei 2017, *ApJ*, 849, 144
- Christensen-Dalsgaard, Jørgen & Berthomieu, Gabrielle 1991, In: *Solar interior and atmosphere*, Tucson, AZ, University of Arizona Press, 401
- Davies, G. R., Chaplin, W. J., Elsworth, Y. P. & Hale, S. J. 2014, *MNRAS*, 441, 3009
- Giles, P. M., Duvall, T. L., Scherrer, P. H., & Bogart, R. S. 1997, *Nature*, 390, 52
- Goldreich, P., Murray, N. & Kumar, P. 1994, *ApJ*, 424, 466
- Gough, D.O. 1990, In: Osaki, Y., Shibahashi, H. (eds.) *Progress of Seismology of the Sun and Stars, Lecture Notes in Physics* 367, Springer, Berlin, 283
- Gizon, Laurent & Birch, Aaron C. 2005, *LRSP*, 2, 6
- Hale, S. J., Howe, R., Chaplin, W. J., Davies, G. R. & Elsworth, Y. P. 2016, *Sol. Phys.*, 291, 1
- Hathaway, David H. 2015, *LRSP*, 12, 4
- Howe, R., Komm, R.W., & Hill, F. 2002, *ApJ*, 580, 1172
- Howe, R., Davies, G. R., Chaplin, W. J., Elsworth, Y., Basu, S., Hale, S. J., Ball, W. H. & Komm, R. W. 2017, *MNRAS*, 470, 1935
- Howe, R., Chaplin, W. J., Davies, G. R., Elsworth, Y., Basu S., & Broomhall, A. -M. 2018, *MNRAS*, 480, L79
- Howe, R., Hill, F., Komm, R., Chaplin, W. J., Elsworth, Y., Davies, G. R., Schou, J. & Thompson, M. J. 2018, *ApJL*, 865, L5
- Keith-Hardy, J. Z., Tripathy, S. C., Jain, K. 2019, *ApJ*, 877, 148
- Kiefer, René, Schad, Ariane & Roth, Markus 2017, *ApJ*, 846, 162
- Kiefer, René & Roth, Markus 2018, *ApJ*, 854, 74

- Kiefer, René, Komm, Rudi, Hill, Frank, Broomhall, Anne-Marie & Roth, Markus 2018, *Sol. Phys*, 293, 151
- Komm, R., Howe, R. & Hill, F. 2018, *Sol. Phys*, 293, 145
- Kosovichev, Alexander G. & Pipin, Valery V. 2019, *ApJL*, 871, L20
- Libbrecht, K.G. & Woodard, M.F. 1990, *Nature*, 345, 779
- Liang, Zhi-Chao, Gizon, Laurent, Birch, Aaron C., Duvall, Thomas L. & Rajaguru, S. P. 2018, *A&A*, 619, 99
- Lund, Mikkel Nørup, Kjeldsen, Hans, Christensen-Dalsgaard, Jørgen, Handberg, Rasmus & Silva Aguirre, Victor 2014, *ApJ*, 782, 2
- Mandal, K., Hanasoge, S. M., Rajaguru, S. P. & Antia, H. M. 2018, *ApJ*, 863, 39
- Mitra-Kraev, U. & Thompson, M. J. 2007, *AN*, 328, 1009
- Parker E. N. 1955, *ApJ*, 122, 293
- Salabert, D., García, R. A. & Turck-Chièze, S. 2015, *A&A*, 578, 137

## Discussion

**KOSOVICHEV:** The p-mode frequency shift varies similarly to the radio flux but there is a significant difference in cycle 24. What can be learned from this difference?

**BROOMHALL:** There does appear to be a change in relationship between the radio flux and the frequency shifts from one cycle to the next. If we plot one against the other, as is done in Figure 6, we can readily see this change. However, we only really have two cycles to compare (three if we use BiSON data) and so, at the moment, it is difficult to determine exactly what causes this change. This behaviour is seen if we compare the frequency shifts to other proxies as well, such as sunspot area, and, similarly, if you compare two non-helioseismic activity proxies. One potential explanation comes in terms of the extent of the near-surface layer responsible for perturbing the mode frequencies. This layer becoming thinner between cycles 23 and 24 would be consistent with the observations. However, I believe more will be revealed as the next cycle progresses.